J Appl Electrochem (2009) 39:879–885
DOI 10.1007/s10800-008-9734-9

ORIGINAL PAPER

Electroless plating of Ni–P coatings on carbon steel in a stirred bed of glass balls

Zhaoxia Ping · Yedong He · Changdong Gu · Tong-Yi Zhang

Received: 10 August 2008 / Accepted: 19 November 2008 / Published online: 9 December 2008

Abstract The electroless plating of Ni–P coatings was carried out in a stirred plating solution containing a bed of glass balls with a fixed stirring rate of 1,800 rpm. The diameters of the glass balls were 2 and 3 mm and the total weight of the balls was ~200 g; the weight ratio of the 2 mm to the 3 mm balls was 3:2. The as-deposited Ni–P coating was composed of fine polycrystalline Ni grains and had a smooth appearance. The hardness and corrosion resistance of the novel coatings were considerably improved compared with the conventional electroless (CE)-plated amorphous Ni–P coatings. After heat treatment at 400 °C for 1 h, cracks occurred in the CE-plated Ni–P coating, while no cracks appeared in the mechanically assisted electroless (MAE)-plated Ni–P coating. These improved properties of the MAE-plated Ni–P coatings demonstrate the advantages of this novel technique, which may find wide application in industry.

Keywords Mechanically assisted electroless plating · Ni–P coating · Crystallization · Corrosion resistance · Microhardness

Z. Ping · Y. He
Beijing Key Laboratory for Corrosion, Erosion and Surface Technology, University of Science and Technology Beijing, 100083 Beijing, China

Z. Ping · T.-Y. Zhang
The Hong Kong–Beijing UST Joint Research Center, HKUST, Fok Ying Tung Graduate School, Nansha, Guangzhou, China

C. Gu · T.-Y. Zhang (✉)
Department of Mechanical Engineering, Hong Kong University of Science and Technology, Hong Kong, China
e-mail: mezhangt@ust.hk

1 Introduction

Electroless-plated nickel–phosphorus (Ni–P) coatings have been widely used in various industries [1–3]. The electroless-plating process and post-plating heat treatment determine the Ni–P coating composition and microstructure; this has attracted intense interest [4–10]. Amorphous Ni–P coatings are formed in electroless-plating when the P content is higher than 8% [11]. If the coatings are crystalline, the mechanical properties are greatly improved [5, 6, 8, 9, 12–14]. Crystallization of amorphous Ni–P coatings is usually achieved by post-plating heat treatment. Due to the mechanical constraints of substrates, residual tensile stresses in Ni–P coatings generally occur during the heat treatment because the specific density of the Ni–P coating in the amorphous phase is smaller than that in the crystalline phase, which might lead to cracking of the coatings if the tensile stresses are larger than a critical value [15]. Cracks would degrade the corrosion resistance of the Ni–P coating and other crack-related mechanical properties [16]. Crystalline Ni–P coatings free of cracks are desired for industrial applications. How to produce the desired Ni–P coatings is a challenging issue. The present study explores a MAE-plating technique to achieve this goal.

Mechanically assisted plating has been much investigated [17–24]. Early study focused on the change in the depletion zone at the deposit surface by a mechanical means [17–21], while recent study concentrates on in-situ mechanical treatments of coatings [22–24]. If an in-situ mechanical treatment can crystallize Ni–P coatings and generate compressive residual stresses with a desired level, the mechanical properties of the coatings will be improved considerably. He et al. [25] report that Ni–P coatings on Mg-alloy plated with mechanical assistance are polycrystalline

with averaged grain size of 27 nm, are crack-free, possess high hardness of 563 HV and have enhanced corrosion resistance. Following previous work, we apply the MAE-plating technique to deposit Ni–P on carbon steel.

2 Experimental procedure

The MAE-plating set-up is schematically shown in Fig. 1. The electroless plating of Ni–P coatings was carried out in a stirred plating solution bed of glass balls with a fixed stirring rate of 1,800 rpm. The ball diameters were 2 and 3 mm and the total weight of the balls was ~200 g; the weight ratio of the 2 mm to the 3 mm balls was 3:2. The present process is similar to that in a fluidised bed of particles [26–29]. During the plating process the glass balls impact or/and roll on the sample being plated. This mechanically assisted plating enhances the coating quality. Each carbon steel sample had dimensions of 20 mm × 10 mm × 2 mm. The sample surfaces were ground with SiC papers to 1200-grit finish. The composition of the plating solution and the plating parameters are listed in Table 1. Before deposition, the sample was first degreased ultrasonically in ethanol for 5 min, rinsed with deionized water, and then immersed in 5% dilute hydrochloric acid for 30–60 s and thoroughly rinsed again with deionized water. MAE-plating and CE-plating were all carried out at 80 °C and each plating process lasted for 1 h. Some plated samples were annealed at 400 °C for 1 h to investigate the cracking phenomenon induced by crystallization.

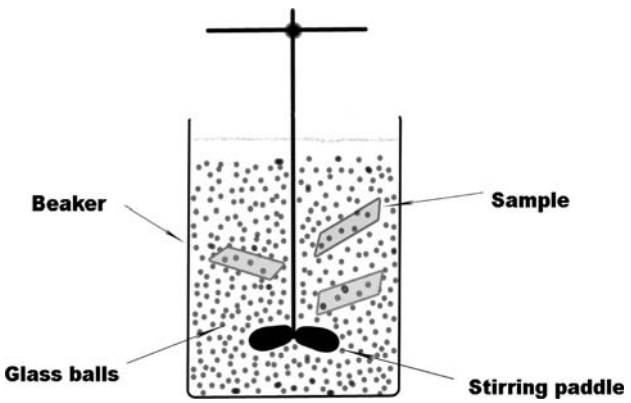

Fig. 1 Schematic diagram of MAE-plating set-up

Table 1 Composition of the plating solution and plating parameters

Plating solution composition		Electroless parameters	
$NiSO_4 \cdot 6H_2O$	25 g L^{-1}	pH	5.5
$NaH_2PO_2 \cdot H_2O$	20 g L^{-1}	Temperature	80 °C
$NaCH_3COO \cdot H_2O$	5 g L^{-1}	Time	1 h
$C_6H_5Na_3O_7 \cdot 2H_2O$	5 g L^{-1}		

X-ray diffraction analysis (XRD, PW3710, Philips) was conducted to characterize crystal structures of the as-deposited coatings and the coatings after heat treatment. The surface and cross-sectional morphologies of coatings were examined by scanning electron microscopy (SEM, JSM-6480LV). Chemical compositions of the coatings were analyzed with an X-ray energy dispersive spectroscope (EDS) attached to the SEM. Hardness of the coatings was measured on the coating surface using a digital microhardness tester (HVS-1000) with a load of 0.49 N and a duration of 20 s. The maximum depth of the indentation impression was about 2 μm, less than 15% of the coating thickness, which ensured that the measured hardness is the coating property. At least 10 indentations were performed to gain the averaged hardness value for each sample.

The anodic polarization and electrochemical impedance spectroscopy (EIS) tests were performed on a galvanochemistry Workstation (CHI660C, Shanghai) in 3.5% NaCl solution at room temperature using a three-electrode electrochemical cell with a platinum plate as the counter-electrode and a saturated calomel electrode (SCE, +242 mV versus NHE) as reference. Each of the samples exposed a test area of 1 cm^2 to the solution and the rest was covered by an anticorrosion tape. The EIS spectra were obtained over the frequency range 10 mHz–100 kHz with an applied AC perturbation potential of 10 mV amplitude. The EIS data were simulated with Boukamp's algorithm implemented in Zsimpwin software. The average surface roughness (Ra) of the as-deposited coatings was determined using an optical profiler (Wyko NT3300, Vecco) in Vertical Scanning Interferometry (VSI) mode. The scanning area and vertical resolution in the VSI mode were 155 × 204 μm^2 and 1 nm, respectively. The surface roughness of the plated coatings was measured in at least five places and the averaged value is reported here.

3 Experimental results

3.1 Surface morphology

Figure 2a–d are SEM pictures, showing surface morphologies of the Ni–P coatings on carbon steel electrolessly plated without and with mechanical assistance, respectively. The MAE-plated Ni–P coating has a much smoother surface than the traditional electroless-plated Ni–P coating. Although both Ni–P coatings exhibit the typical "cauliflower-like" surface, the size of the "cauliflower-like" clusters is below 200 nm on the MAE-plated Ni–P coating surface, while it is about 5–20 μm on the electroless-plated

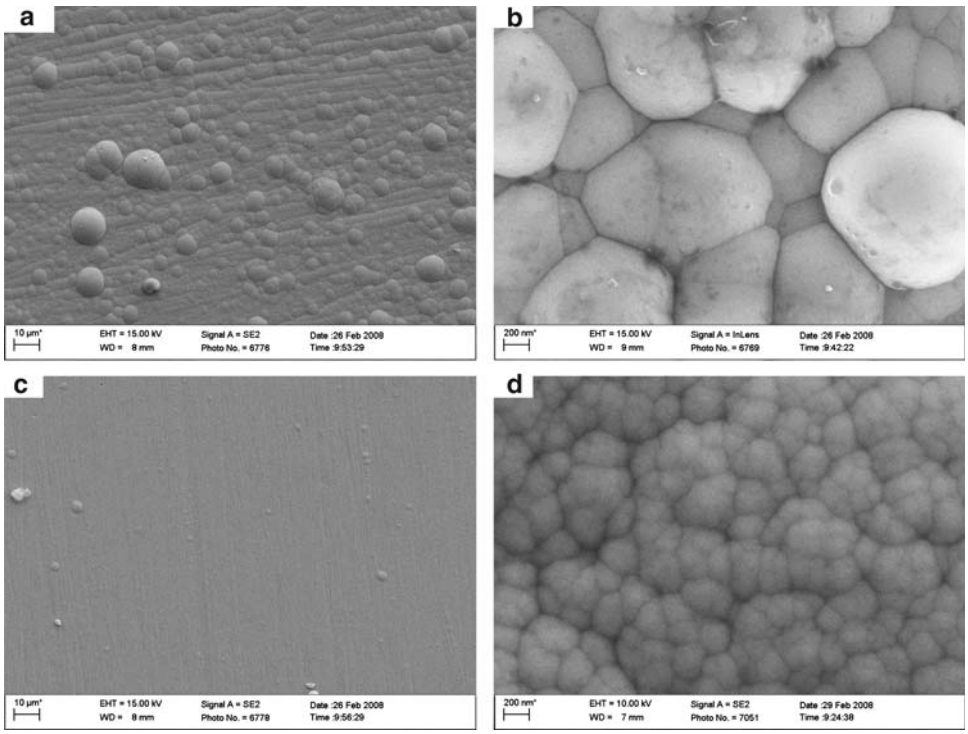

Fig. 2 Surface morphologies of Ni–P coatings on carbon steels electroplated **a**, **b** without and **c**, **d** with mechanical assistance

Ni–P coating surface. The average surface roughness (Ra) of the MAE-plated coating is about 82.88 nm, which is much smaller than that of the CE-plated coating (307.89 nm). The MAE-plating process makes the coating surface smoother.

After heat treatment at 400 °C for 1 h, the surface morphology is much different, as shown in Fig. 3a–d between the CE-plated coatings and the MAE-plated coatings. Cracks appear on the surface of the CE-plated coatings, while no cracks are found on the surface of the

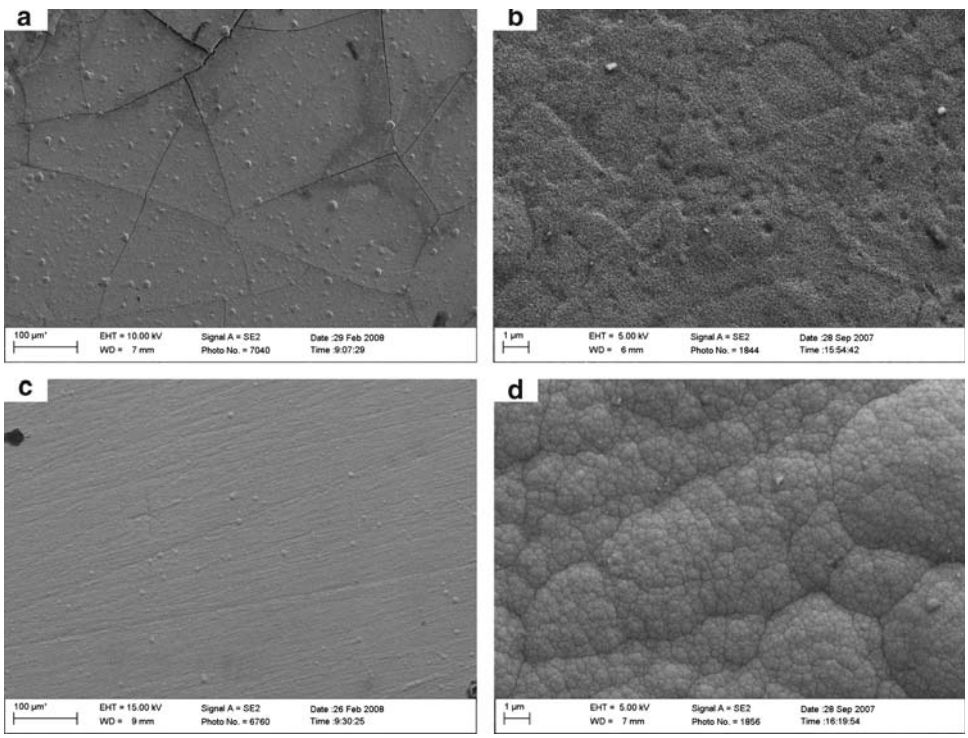

Fig. 3 Surface morphologies of **a**, **b** electroless plated and **c**, **d** MAE plated Ni–P coatings on carbon steels after heat treatment at 400 °C for 1 h

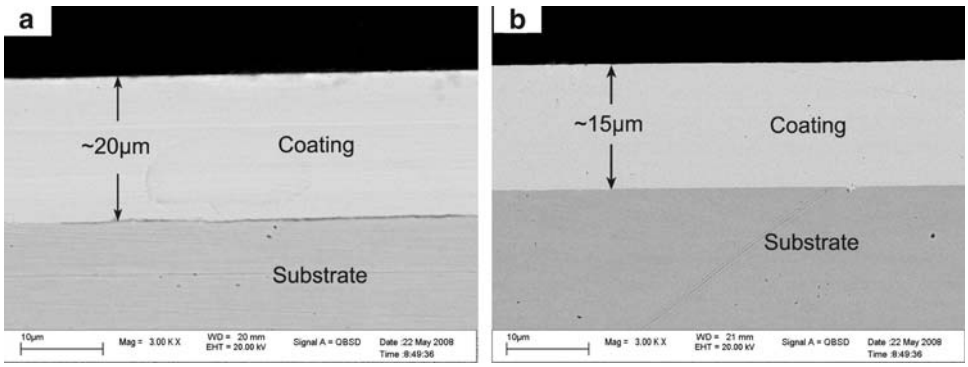

Fig. 4 Cross-section SEM images of Ni–P coatings on carbon steel **a** by CE-plating and **b** by MAE-plating

MAE-plated Ni–P coatings. Crystallization of amorphous Ni–P coatings is usually achieved by post-plating heat treatment. Because the specific density of the Ni–P coating in the amorphous phase is smaller than that in the crystalline phase [15], tensile residual stresses in the Ni–P coatings are generated by the crystallization treatment. Tensile residual stresses may cause cracking of Ni–P coatings or not [30], depending on coating and heat treatment conditions. Nevertheless, tensile residual stresses in the Ni–P coatings are the driving force to cause potential damage of the coatings in service. In addition to cracks, small pores are formed in the CE-plated Ni–P coating, as shown in Fig. 3b. No pores are observed in the SEM image of Fig. 3d on the surface of the MAE-plated Ni–P coating. Comparing Fig. 3d with Fig. 2d indicates that the surface morphology of the MAE-plated Ni–P coating remains almost unchanged after heat treatment. The MAE-plating technique solves the severe cracking problem of Ni–P coatings.

Figure 4a and b are SEM images of the cross-section of the Ni–P coatings produced by electroless-plated without and with mechanical assistance, respectively. Under the same plating condition, the thickness of the CE-plated coating is about 20 μm, whereas the thickness of the MAE-plated Ni–P coating is about 15 μm. Mechanical in-situ treatment makes the Ni–P coating become thinner by about 5 μm. In addition, the interface roughness between the carbon steel substrate and the Ni–P coating is reduced by the mechanical in-situ treatment.

3.2 Composition and phase analysis

EDS analysis indicates that the P content is about 13 wt% in the CE-plated Ni–P coating and about 11.2 wt% in the MAE-plated Ni–P coating. When the P content is higher than 8% [11], Ni–P coatings are usually amorphous. As expected, the CE-plated Ni–P coating without heat treatment is amorphous, as proved by the XRD pattern (see Fig. 5a). The MAE-plating produces crystalline Ni–P coating, as evidenced by the XRD pattern (see Fig. 5b),

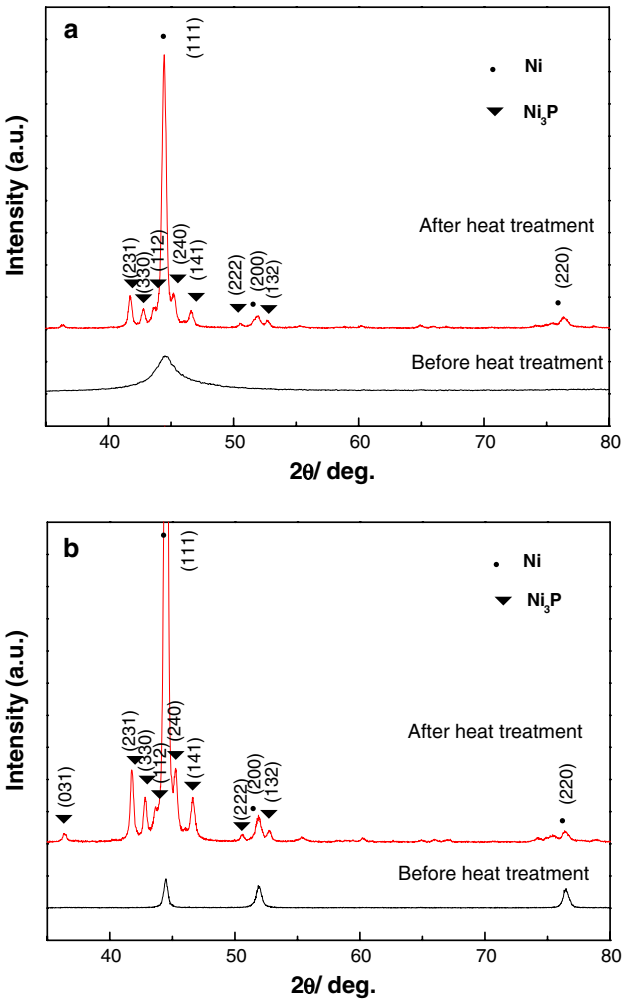

Fig. 5 Comparison of XRD patterns for **a** electroless-plated Ni–P coating and **b** MAE-plated Ni–P coating before the heat treatment and after

where only the face-centered cubic (fcc) Ni peaks are visible. After heat treatment, the traditional electroless plated Ni–P coating and the electroless-plated with mechanical assistance Ni–P coating are fully crystallized into Ni and Ni_3P phases, as shown in Fig. 5a and b. The

heat treatment induced crystallization of Ni–P coatings is similar to that reported elsewhere [31].

3.3 Microhardness

The microhardness test results show that the CE-plated and MAE-plated Ni–P coatings have mean microhardnesses of 430 ± 10 HV and 567 ± 12 HV, respectively. The mechanical in-situ treatment increases the microhardness of the Ni–P coating by about 137 HV, thereby indicating that the wear resistance of the Ni–P coating will be greatly improved. After heat treatment, the microhardnesses of CE-plated Ni–P coating is 670 ± 10 HV and the MAE-plated Ni–P coating is increased to 860 ± 10 HV. The average grain size, d, of Ni and Ni_3P crystals may be estimated from the full width of half maximum (FWHM) of a XRD peak via the Scherrer equation [32]:

$$d_{\mathrm{XRD}} = \frac{k\lambda}{\beta(\theta)\cos\theta} \quad (1)$$

where λ is the X-ray wavelength, β the FWHM of the diffraction peak, θ the diffraction angle and the constant $k \approx 1$. From the XRD patterns indicated in Fig. 5a and b and using Eq. 1, we estimate the average grain sizes of Ni and Ni_3P in the MAE-plated Ni–P coating to be 28 and 32 nm, respectively, which are correspondingly smaller than the average grain sizes of Ni and Ni_3P in the CE-plated Ni–P coating, 320 nm for Ni and 210 nm for Ni_3P. This may be the reason why the MAE-plated Ni–P coating after heat treatment exhibits enhanced microhardness compared with the CE-plated Ni–P coating after the same annealing process.

3.4 Electrochemical testing

Figure 6 shows polarization curves of the CE-plated Ni–P coatings and MAE-plated Ni–P coatings before and after heat treatment, and the carbon steel substrate in 3.5% NaCl solution at room temperature. The carbon steel has the most negative corrosion potential E_{corr} among the studied samples. Before heat treatment, the E_{corr} of the MAE-plated Ni–P coating is higher than that of the CE-plated Ni–P coating. After heat treatment, the E_{corr} of the MAE-plated Ni–P coating is also higher than that of the CE-plated Ni–P coating. This indicates that the corrosion resistance of the Ni–P coating is improved by the mechanical in-situ treatment. After the heat treatment, corrosion potentials of the CE-plated coating and the MAE-plated coating both shift negatively in comparison with the original values before heat treatment. The negative shift in corrosion potential may be attributed to stresses induced by the crystallization heat treatment.

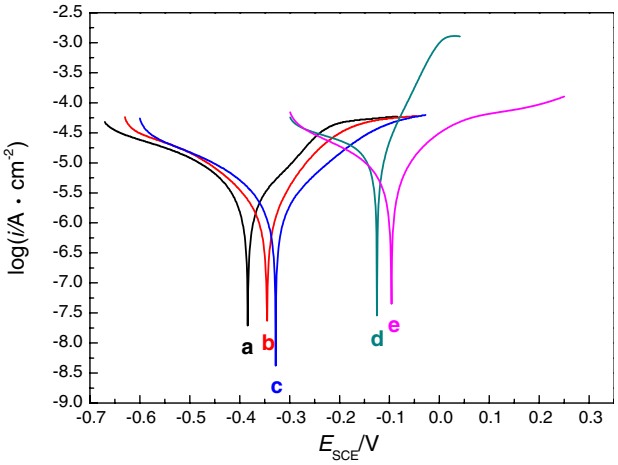

Fig. 6 Polarization curves in 3.5% NaCl solution at room temperature: (a) carbon steel substrate; (b) CE-plated coating after heat treatment; (c) CE-plated coating before heat treatment; (d) MAE-plated coating after heat treatment and (e) MAE-plated coating before heat treatment

The measured EIS data in the Nyquist format are presented in Fig. 7a. Figure 7b shows an equivalent circuit, which consists of a solution resistance (R_S), a constant-phase element (Q_{dl}), a polarization resistance (R_t) and a Warburg component (W). The Warburg impedance is

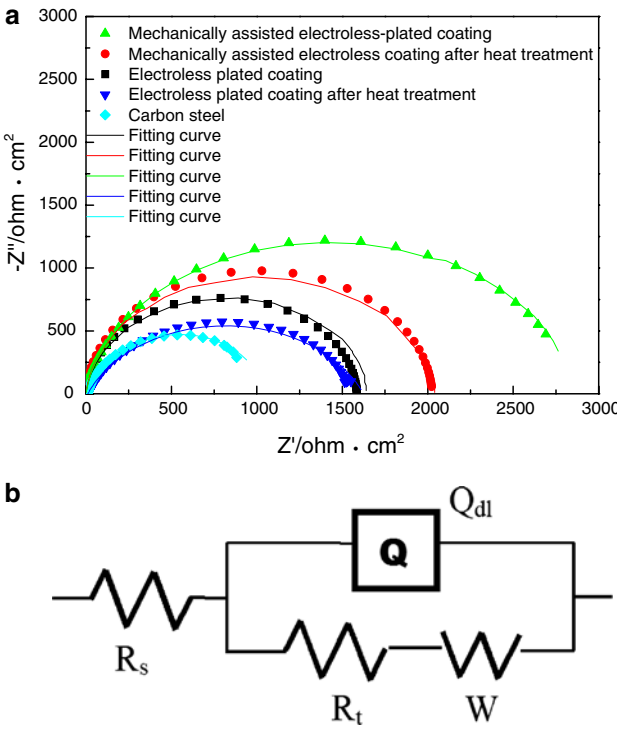

Fig. 7 **a** Nyquist plots for carbon steel substrate, conventional and MAE-plated Ni–P coatings before the heat treatment and after in 3.5% NaCl solution at room temperature, respectively. **b** Equivalent circuit for fitting the EIS data

Table 2 The fitting result of EIS of the carbon steel, the electroless-plated Ni–P coating and the MAE-plated Ni–P coating

Sample	R_s (Ω cm^2) (%)	R_{ct} (Ω cm^2) (%)	Q_{dl} (F cm^{-2}) (%)	n_{dl} (%)	W (%)
Carbon steel	3.389 ± 1	1066 ± 2	7.244E−4 ± 0.3	0.7852 ± 1.2	6.317E19 ± 12
CE-plated Ni–P coating after heat treatment	3.47 ± 1.3	1582 ± 2.6	1.086E−4 ± 0.2	0.9757 ± 1.4	1.256E8 ± 10
CE-plated Ni–P coating before heat treatment	3.50 ± 1.6	1614 ± 3	1.106E−4 ± 1	0.7514 ± 1.7	1.561E8 ± 11
MAE-plated Ni–P coating after heat treatment	0.9136 ± 1	2025 ± 2.1	1.742E−4 ± 0.4	0.9782 ± 1.5	2.717E11 ± 15
MAE-plated Ni–P coating before heat treatment	1.088 ± 1	2187 ± 2	2.127E−5 ± 1	0.9876 ± 1	8.8884E4 ± 17

usually observed at low frequencies in electrochemical experiments due to the concentration polarization induced by a sluggish diffusion process. The circuit parameters were approximately determined by fitting the experimental data with the equivalent circuit and tabulated in Table 2. In Table 2, factor n_{dl} represents the Q_{dl} power, which is usually between 0.5 and 1 [33]. When $n_{dl} = 1$, a Q_{dl} is equivalent to an ideal capacitor. The EIS analysis shows that the polarization resistance (R_t) of the MAE-plated Ni–P coating is higher than that of the CE-plated Ni–P coating, thereby indicating again that the corrosion resistance is improved by the mechanical in-situ treatment. After the heat treatment, the values of R_t are decreased slightly for both conventional electroless-plated coating and MAE-plated coating, which is consistent with the negative shift of the corrosion potential.

4 Discussion

Amorphous alloys are of meta-stable phases in a thermodynamic sense and may be crystallized to reach the equilibrium state through annealing. Amorphous Ni–P coating is crystallized to fcc Ni and tetragonal Ni_3P phases after heat treatment at 400 °C for 1 h [34]. The as-prepared Ni–P coating produced by MAE-plating includes Ni polycrystals without the precipitation of Ni_3P phase, which indicates that the energy supplied by in-situ mechanical treatment during deposition could induce partial crystallization of the amorphous phase. When Ni and P atoms are deposited on the substrate at room temperature the meta-stable amorphous state may be at the local energy minimum so that the CE-plated Ni–P coating is amorphous. In addition, the surface diffusion of Ni and P atoms may play a critical role in the formation of the amorphous coating. Under the CE-plating condition, the mobility of deposited Ni and P atoms may be too low and unable to overcome the energy barrier for crystallization. With the mechanical in-situ treatment, the balls impact on the deposited coating and exert a mechanical force on the coating. Under such in-situ mechanical force, the energy barrier for crystallization is greatly reduced. The detailed thermodynamic analysis is reported in a previous publication [35]. The incomplete crystallization and the lack of Ni_3P phase in as-deposited coating electroless-plated with the mechanical in-situ assistance may indicate that the mobility of Ni and P atoms might not be enhanced too much by the mechanical in-situ treatment.

After heat treatment, cracks are observed in the CE-plated Ni–P coating, indicating that a tension stress field is built up. This means that volume shrinkage during crystallization of the amorphous coating occurs. Since the MAE-plated Ni–P coating has been crystallized, its density must be higher than that of the CE-plated coating. Therefore, the volume change during the heat treatment must be much smaller in the MAE-plated Ni–P coating than that in the CE-plated coating so that no cracking occurs. After heat treatment, as described above, the grain sizes of Ni and Ni_3P in the MAE-plated Ni–P coating are all smaller than those in the CE-plated coating. Thus, the hardness, corrosion resistance and wear resistance are greatly improved by the mechanical in-situ treatment.

5 Conclusions

A novel coating process—MAE-plating—has been developed to deposit Ni–P coatings on carbon steel. The Ni–P coatings possess smooth surfaces and a fine grained structure. The coating properties including hardness and corrosion resistance are improved. No cracks in the MAE-plated Ni–P coatings are formed after heat treatment at 400 °C for 1 h. These excellent properties produced by the mechanical in-situ treatment may produce wide application of the MAE-plating technique in engineering practice.

Acknowledgments The work was financially supported by the Chinese National Nature Science Foundation (Grant.50671006). Zhaoxia Ping was partially supported by the Fok Ying Tung Graduate School, HKUST.

References

1. Baudrand DW (1994) ASM handbook, vol 5. ASM International, Materials Park, p 290
2. Zhang YZ, Yao M (1999) Trans Inst Met Finish 77(2):78

3. Tummala RR, Rymaszeski EJ, Klopfenstein AG (1997) Microelectronics packaging handbook—part 2, chap 8. Chapman and Hall, London
4. Tyagi SVS, Barthwal SK, Tandon VK, Ray S (1989) Thin Solid Films 169(2):229
5. Kumar PS, Nair PK (1996) J Mater Process Technol 56:511
6. Martyak NM, Drake K (2000) J Alloy Compd 312:30
7. Ma EM, Luo SF, Li PX (1988) Thin Solid Films 166:273
8. Agarwala RC, Ray S (1989) Z Metallkd 80(8):556
9. Hur KH, Jeong JH, Lee DN (1991) J Mater Sci 26(8):2037
10. Parker K (1981) Plat Surf Finish 68(12):71
11. Goldenstein AW, Rostoker W, Schossberger F (1957) J Electrochem Soc 2:104
12. Tyagi SVS, Barthwal SK, Tandon VK, Ray S (1989) Thin Solid Films 169:229
13. Narayan R, Mungole MN (1985) Met Finish 83:55
14. Staia MH, Cadtillo EJ, Puchi ES, Hintermann HE (1996) Surf Coat Technol 86–87:598
15. Song JY, Yu J (2002) Thin Solid Films 415:167
16. Razavi R Sh, Salehi M, Monirvaghefi M, Gordani GR (2008) J Mater Process Technol 195:154
17. Eisner S (1971) J Plat (USA) 58:993
18. Wisdom NE, Eisner S (1971) J Plat (USA) 58:1099
19. Eisner S, Wisdom NE (1971) J Plat (USA) 58:1183
20. Eisner S (1972) US Patent 3,753,889
21. Eisner S, Trans J (1973) Met Finish 51:13
22. He YD, Zhan ZL, Wang DR Chinese patent ZL200410009189.7
23. Zhan ZL, He YD, Wang DR, Gao W (2006) J Intermet 14:75
24. Ning Z, He Y, Gao W (2008) Surf Coat Technol 202:2139
25. He Y, Fu H, Li X, Gao W (2008) Scr Mater 58:504
26. Germain S, Goodridge F (1976) Electrochim Acta 21:545
27. Fleischm M, Oldfield JW (1971) J Electroanal Chem 29:211
28. Fleischm M, Oldfield JW (1971) J Electroanal Chem 29:231
29. Fleischm M, Oldfield JW, Porter DF (1971) J Electroanal Chem 29:241
30. Keong KG, Sha W, Malinov S (2003) Surf Coat Technol 168:263
31. Keong KG, Sha W, Malinov S (2002) J Alloy Compd 334:192
32. Birks LS, Friedman H (1946) J Appl Phys 17:687
33. Guo Z, Keong KG, Sha W (2003) J Alloy Compd 358:112
34. Keong KG, Sha W, Malinov S (2002) J Mater Sci 37:4445
35. Ping Z, He Y, Gu C, Zhang T (2008) Surf Coat Technol 202:6023